Intensity of Singular Stress Fields at the End of a Cylindrical Inclusion

N.-A. Noda

T. Genkai

Q. Wang

Mechanical Engineering Department,
Kyushu Institute of Technology,
Kitakyushu 804-8550, Japan

In short fiber reinforced composite it is known that the singular stress at the end of fibers causes crack initiation, propagation, and final failure. The singular stress field is controlled by the generalized stress intensity factors defined at the end of the inclusion. In this study the stress intensity factors are discussed for an elastic cylindrical inclusion in an infinite body under (A) asymmetric uniaxial tension in the x direction, and (B) symmetric uniaxial tension in the z direction. These problems are formulated as a system of integral equations with Cauchy-type or logarithmic-type singularities, where densities of body force distributed in infinite bodies having the same elastic constants as those of the matrix and inclusion are unknown. In the numerical analysis, the unknown body force densities are expressed as fundamental density functions and weight functions. Here, fundamental density functions are chosen to express the symmetric and skew-symmetric stress singularities. Then, the singular stress fields at the end of a cylindrical inclusion are discussed with varying the fiber length and elastic ratio. The results are compared with the ones of a rectangular inclusion under longitudinal and transverse tension.
[DOI: 10.1115/1.1598479]

1 Introduction

In short fiber reinforced composite it is known that the singular stress at the end of fibers causes crack initiation, propagation, and final failure. Recently, Chen and Nisitani [1,2] indicated that the singular stress field is controlled by the generalized stress intensity factors (SIF's) defined for inclusion corners, and Chen [3,4] discussed the singular stress of a rectangular inclusion as a two-dimensional (2D) model. Since actual fibers always have 3D shapes and dimensions, 3D analysis is necessary to evaluate the strength of composites. From this viewpoint, a cylindrical inclusion is important as a 3D model of a fiber in matrix. In previous studies, Kasano et al. [7] treated a rigid cylindrical inclusion, and Hasegawa and Yoshiya [8] solved an elastic cylindrical inclusion with rounded ends. Takao et al. [9], Hasegawa et al. [10], and Wu and Du [11,12] discussed stress fields induced by uniform eigenstrain given within a cylindrical domain. Usually to obtain generalized SIF's for 3D problems is more difficult than to obtain normal SIF's defined for ordinal cracks. Therefore, when Chen and Nisitani [3–5] applied the body force method [6] to 2D problems, they examined two types of numerical procedures, one of which is obtained from the values of unknown body force densities, and the other of which is from the values of stress around the inclusion corner. In both procedures the final results were extrapolated from the results of finite numbers of collocation points [4–6].

In this study the stress intensity factors are discussed for an elastic cylindrical inclusion in an infinite body under (A) asymmetric uniaxial tension in the x direction, and (B) symmetric uniaxial tension in the z direction. The asymmetric problem (A) is solved on the superposition of two auxiliary loads; (i) biaxial tension and (ii) plane state of pure shear. Those problems are formulated as a system of integral equations with Cauchy-type or logarithmic-type singularities, where densities of body force distributed in infinite bodies having the same elastic constants as those of the matrix and inclusion are unknown. In the numerical analysis, the unknown functions of the body force densities are expressed as fundamental density functions and weight functions. Here, the weight functions are approximated as power series instead of step or linear functions used usually in the body force method [3–6]. Then, the singular stress fields at the end of a cylindrical inclusion are discussed for the wide range of the fiber length and elastic ratio.

Contributed by the Applied Mechanics Division of THE AMERICAN SOCIETY OF MECHANICAL ENGINEERS for publication in the ASME JOURNAL OF APPLIED MECHANICS. Manuscript received by the ASME Applied Mechanics Division, July 30, 1999; final revision, Jan. 16, 2003. Associate Editor: J. W. Ju. Discussion on the paper should be addressed to the Editor, Prof. Robert M. McMeeking, Department of Mechanical and Environmental Engineering University of California—Santa Barbara, Santa Barbara, CA 93106-5070, and will be accepted until four months after final publication of the paper itself in the ASME JOURNAL OF APPLIED MECHANICS.

2 Theory and Solution

Consider a cylindrical bar in an infinite body under asymmetric uniaxial tension in the x direction shown in Fig. 1*a*. This problem is composed of the superposition of two auxiliary loads; biaxial tension in the xy plane, shown in Fig. 1*c*, and pure shear in the xy plane, shown in Fig. 1*d*. The method of analysis will be explained for the problem of pure shear in the xy plane. Here, L and D are dimensions of the inclusion, and σ^{∞} is a stress at infinity. The notations (G_M, ν_M) denote the shear modulus and Poisson's ratio of the matrix, and (G_I, ν_I) denotes the ones of the inclusion. Rectangular coordinate (x,y,z) and cylindrical coordinate (r,θ,z) are defined in Fig. 1. Here, (ξ,η,ζ), (ρ,ϕ,ζ) are rectangular and cylindrical coordinates where body forces are applied. The body force method [6] is used to formulate the problem as a system of singular integral equations. Here, the fundamental solutions are stress and displacement fields when two ring forces acting symmetrically to the plane $z=0$. In this case the boundary conditions only on $z \geq 0$ can be considered due to symmetry. The two ring forces have three types [13,14], that is, (1) ring forces in the r direction with the magnitude of $\cos 2\phi$, (2) ring forces in the θ direction with the magnitude of $\sin 2\phi$, (3) ring forces in the z direction with the magnitude of $\cos 2\phi$. In the following discussion, how to satisfy the boundary conditions around corner A will be explained.

The problem can be expressed by the following equations in terms of the unknown body force densities $(F_{nM}, F_{tM}, F_{\theta M})$ and $(F_{nI}, F_{tI}, F_{\theta I})$ distributed at infinitesimal area $\rho d\theta dr_A$ in infinite bodies M and I. Here, bodies M and I have the same elastic constants as those of the matrix and inclusion, respectively, and r_A is a distance from the corner A as shown in Fig. 1*e*. In the following equation, the notation $\int_L$ means integrating body forces on both the side and ends of the cylinder. Here, for example, the notation

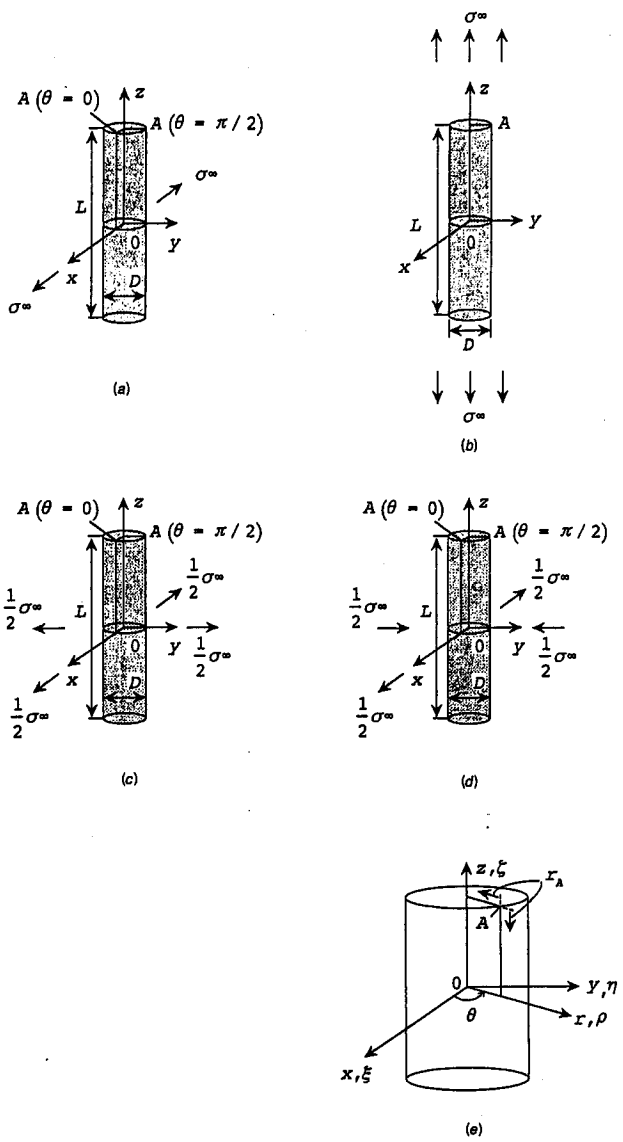

Fig. 1 Problem and coordinate system: (a) Uniaxial tension perpendicular to the axis of the inclusion (*x* direction); (b) Uniaxial tension in the axis of the inclusion (*z* direction); (c) Hydrostatic tension in a plane perpendicular to the axis of the inclusion (*xy* plane); (d) Pure shear in a plane perpendicular to the axis of the inclusion (*xy* plane); (e) Coordinate system

$h_{nn}^{F_{nM}}(r_A,s)$ denotes the normal stress induced at the collocation point s induced by the body force F_{nM} acting at the point r_A. Since the integral includes the Cauchy-type or logarithmic-type singularities, the integration should be interpreted in the Cauchy principal value sense,

$$-\frac{1}{2}F_{nM}(s)-\frac{1}{2}F_{nI}(s)+\int_L h_{nn}^{F_{nM}}(r_A,s)F_{nM}(r_A)dr_A + \int_L h_{nn}^{F_{tM}}(r_A,s)F_{tM}(r_A)dr_A+\int_L h_{nn}^{F_{\theta M}}(r_A,s)F_{\theta M}(r_A)dr_A - \int_L h_{nn}^{F_{nI}}(r_A,s)F_{nI}(r_A)dr_A-\int_L h_{nn}^{F_{tI}}(r_A,s)F_{tI}(r_A)dr_A - \int_L h_{nn}^{F_{\theta I}}(r_A,s)F_{\theta I}(r_A)dr_A = -\{\sigma_{nM}^{\infty}(s)-\sigma_{nI}^{\infty}(s)\}\cos 2\theta, \quad (1a)$$

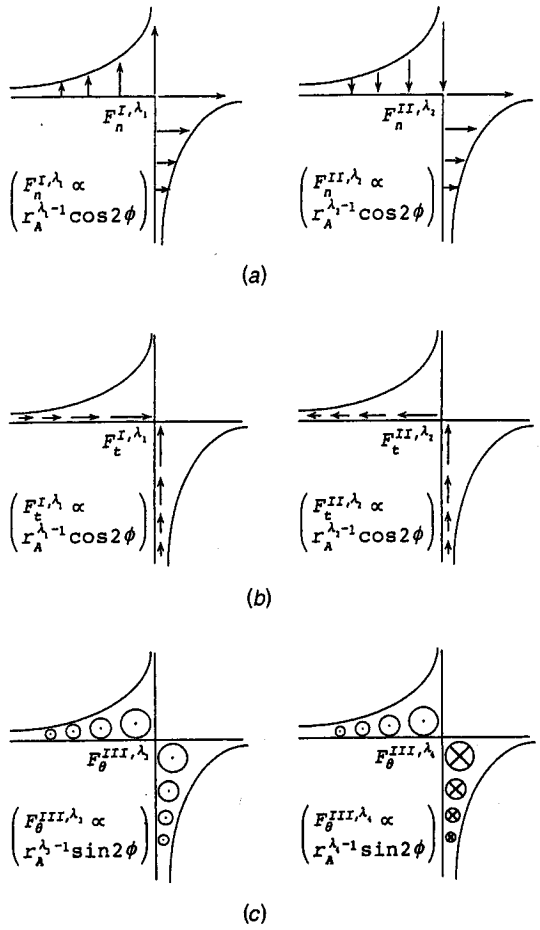

Fig. 2 Two types of body force distributed around the corner in the (*a*) normal, (*b*) tangential, and (*c*) circumferential directions

$$\int_L h_v^{F_{nM}}(r_A,s)F_{nM}(r_A)dr_A+\int_L h_v^{F_{tM}}(r_A,s)F_{tM}(r_A)dr_A + \int_L h_v^{F_{\theta M}}(r_A,s)F_{\theta M}(r_A)dr_A-\int_L h_v^{F_{nI}}(r_A,s)F_{nI}(r_A)dr_A - \int_L h_v^{F_{tI}}(r_A,s)F_{tI}(r_A)dr_A-\int_L h_v^{F_{\theta I}}(r_A,s)F_{\theta I}(r_A)dr_A = -(u_{\theta M}^{\infty}-u_{\theta I}^{\infty})\sin 2\theta. \quad (1b)$$

Equations (1*a*) and (1*b*) enforce the boundary conditions $\sigma_{nM}-\sigma_{nI}=0$, and $u_{\theta M}-u_{\theta I}=0$, respectively; other boundary conditions, that is, $\tau_{ntM}-\tau_{ntI}=0$, $\tau_{n\theta M}-\tau_{n\theta I}=0$, $u_{rM}-u_{rI}=0$, $u_{zM}-u_{zI}=0$, can be expressed in a similar way. In Eqs. (1*a*) and (1*b*) σ_{nM}^{∞} and $u_{\theta M}^{\infty}$ are stress and displacement components induced by the stress at infinity σ^{∞}; here we assume body *I* is also under the stresses $(\sigma_{rI}^{\infty},\sigma_{\theta I}^{\infty},\tau_{r\theta I}^{\infty})$, which induce σ_{nI}^{∞}, and $u_{\theta I}^{\infty}$ in Eqs. (1*a*) and (1*b*).

The singular stress fields near corner A can be expressed by two types of body force distributions; symmetric and skew-symmetric types to the bisector of the corners. Figure 2 indicates the two types of body forces distributed in the normal, tangential, and circumferential directions to the boundary. In the vicinity of corner A, plain strain condition can be assumed; then, the eigenvalues λ_1, λ_2, λ_3, λ_4 controlling the singular stress fields is determined from the eigenequations for 2D problems [1,2,15]. In this study

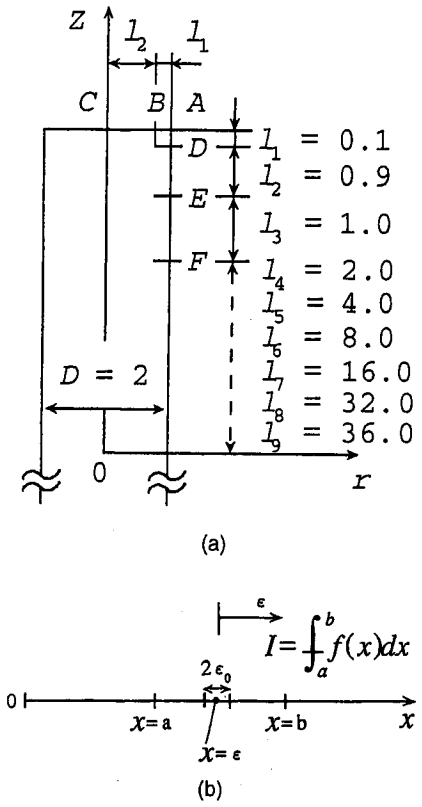

Fig. 3 (*a*) **Typical boundary division for Eqs. (3) and (4).** (*b*) **Boundary division for singular integrals.**

therefore unknown body force densities $F_{n,M}(r_A)\sim F_{\theta,M}(r_A)$ in body M and $F_{n,I}(r_A)\sim F_{\theta,I}(r_A)$ in body I are approximated by using fundamental densities $r_A^{\lambda_1-1}\sim r_A^{\lambda_4-1}$ and weight functions $W_{n,M}\sim W_{\theta,I}^{III,\lambda_4}$, where unknown constants are $a_{n,M}\sim f_{n,I}$,

$$F_{n,j}(r_A)=F_{n,j}^{I,\lambda_1}(r_A)+F_{n,j}^{II,\lambda_2}(r_A)=W_{n,j}^{I}(r_A)r_A^{\lambda_1-1}+W_{n,j}^{II}(r_A)r_A^{\lambda_2-1}$$
$$F_{t,j}(r_A)=F_{t,j}^{I,\lambda_1}(r_A)+F_{t,j}^{II,\lambda_2}(r_A)=W_{t,j}^{I}(r_A)r_A^{\lambda_1-1}+W_{t,j}^{II}(r_A)r_A^{\lambda_2-1} \quad (2)$$

$$F_{\theta,j}(r_A)=F_{\theta,j}^{III,\lambda_3}(r_A)+F_{\theta,j}^{III,\lambda_4}(r_A)=W_{\theta,j}^{III,\lambda_3}(r_A)r_A^{\lambda_3-1}+W_{\theta,j}^{III,\lambda_4}(r_A)r_A^{\lambda_4-1} \quad (j=M,I),$$

$$W_{n,j}^{I,\lambda_1}(r_A)=\sum_{n=1}^{M} a_{n,j}r_A^{n-1},$$

$$W_{t,j}^{I,\lambda_1}(r_A)=\sum_{n=1}^{M} b_{n,j}r_A^{n-1}, \quad W_{\theta,j}^{III,\lambda_3}(r_A)=\sum_{n=1}^{M} c_{n,j}r_A^{n-1}, \quad (3)$$

$$W_{n,j}^{II,\lambda_2}(r_A)=\sum_{n=1}^{M} d_{n,j}r_A^{n-1},$$

$$W_{t,j}^{II,\lambda_2}(r_A)=\sum_{n=1}^{M} e_{n,j}r_A^{n-1},$$

$$W_{\theta,j}^{III,\lambda_4}(r_A)=\sum_{n=1}^{M} f_{n,j}r_A^{n-1} \quad (j=M,I).$$

Here, fundamental density functions are chosen to express the symmetric stress singularity of the forms $1/r^{1-\lambda_1}$, $1/r^{1-\lambda_3}$ and the skew-symmetric stress singularity of the forms $1/r^{1-\lambda_2}$, $1/r^{1-\lambda_4}$. Equations (2) and (3) do not include the terms expressing local

Table 1 Convergence of F_{I,λ_1}, F_{II,λ_2}, F_{III,λ_3} ($L/D=10$, $G_I/G_M=10^2$, $\nu_I=\nu_M=0.3$)

M	F_{I,λ_1}			F_{II,λ_2}			F_{III,λ_3}
	from $W_{nH}^{I}(0)$	from $W_{tM}^{I}(0)$	Average	from $W_{nH}^{II}(0)$	from $W_{tM}^{II}(0)$	Average	from $W_{\theta H}^{III}(0)$
2	0.290	0.417	0.354	-0.723	-0.763	-0.743	0.070
3	0.321	0.396	0.359	-0.792	-0.795	-0.794	0.027
4	0.333	0.388	0.361	-0.790	-0.789	-0.789	0.019
5	0.338	0.383	0.360	-0.788	-0.788	-0.788	0.014
6	0.340	0.379	0.360	-0.789	-0.788	-0.789	0.011

uniform streching and shear distortion at corner A. Therefore the stresses $(\sigma_{rI}^{\infty},\sigma_{\theta I}^{\infty},\tau_{r\theta I}^{\infty})$ applied in body I. In the numerical calculation, we may set the values of $(\sigma_{rI}^{\infty},\sigma_{\theta I}^{\infty},\tau_{r\theta I}^{\infty})$ in body I so as to produce the same strains appearing in body M under the stress σ^{∞}. The eigenvalues λ_1, λ_2 are given as the roots of the eigenequations for in-plane deformation [15,2], and the eigenvalues λ_3, λ_4 are given as the roots of the eigenequations for antiplane deformation [1]. For example, the eigenequations for antiplane deformation are shown in Eqs. (4) and (5).

For a symmetric state of stress singularity,

$$\frac{\sin\lambda(\gamma-\pi)}{\sin\lambda\pi}=+\frac{\Gamma+1}{\Gamma-1}. \quad (4)$$

For a skew-symmetric state of stress singularity,

$$\frac{\sin\lambda(\gamma-\pi)}{\sin\lambda\pi}=-\frac{\Gamma+1}{\Gamma-1}, \quad (5)$$

where the corner angle for matrix $\gamma=3\pi/2$ and the elastic ratio $\Gamma=G_M/G_I$. When $G_M>G_I$, there is a real root λ_3 of Eqs. (4), but no roots λ_4 of Eqs. (5). On the contrary, when $G_M<G_I$, there is a real root λ_4 of Eqs. (4), but no roots λ_3 of Eqs. (5).

Figure 3*a* illustrates an example of boundary divisions for $L/D=10^2$. In the numerical solutions for elliptical inclusions, we do not have to divide the boundaries because the "fundamental densities" to express an elliptical inclusion exactly are available [16]. On the other hand, the boundary division is introduced here because in this problem the fundamental densities are only useful near the corner. Then, the fundamental densities with singularities of symmetric and skew-symmetric types are employed on boundaries C-B-A-D-E in Fig. 3. It is confirmed that the results are not affected until almost to the third digit by changing a region over which the fundamental densities are used. Except along the boundaries C-B-A-D-E in Fig. 3, body forces are simply distributed in the normal, circumferential, and tangential directions without using symmetric and skew-symmetric distributions. On the numerical solution as shown in Eqs. (2) and (3), the singular integral Eqs. (1*a*) and (1*b*) are reduced to algebraic equations for the determination of the unknown coefficients, for example, $a_{n,M}\sim f_{n,I}$ in Eq. (3). These coefficients are determined from the boundary conditions at suitably chosen collocation points. The

Table 2 Convergence of F_{I,λ_1}, F_{II,λ_2}, F_{III,λ_4} ($L/D=10$, $G_I/G_M=10^{-5}$, $\nu_I=\nu_M=0.3$)

M	F_{I,λ_1}			F_{II,λ_2}			F_{III,λ_4}
	from $W_{nH}^{I}(0)$	from $W_{tM}^{I}(0)$	Average	from $W_{nH}^{II}(0)$	from $W_{tM}^{II}(0)$	Average	from $W_{\theta H}^{III}(0)$
2	0.191	0.221	0.206	1.260	0.989	1.125	0.044
3	0.212	0.227	0.220	1.123	1.024	1.074	0.021
4	0.214	0.223	0.219	1.058	1.051	1.055	0.014
5	0.215	0.222	0.219	1.060	1.048	1.054	0.010
6	0.216	0.221	0.219	1.056	1.047	1.052	0.008

Table 3 F_{I,λ_1} and F_{II,λ_2} for a cylindrical inclusion under uniaxial tension in the z direction ($\nu_I=\nu_M=0.3$)

L/D \ G_I/G_M	F_{I,λ_1}						F_{II,λ_2}					
	10^{-5}	10^{-2}	10^{-1}	2	10^{1}	10^{2}	10^{-5}	10^{-2}	10^{-1}	2	10^{1}	10^{2}
$10^{0.0}=1.0$	0.393	0.374	0.281	0.219	0.292	0.322	1.652	1.687	1.935	3.000	0.624	0.549
$10^{0.5}=3.162$	0.382	0.366	0.278	0.249	0.437	0.659	1.616	1.641	1.877	2.776	0.891	0.959
$10^{1.0}=10.0$	0.379	0.363	0.277	0.255	0.599	1.298	1.604	1.627	1.862	2.780	1.087	1.816
$10^{1.5}=31.62$	0.379	0.363	0.276	0.255	0.618	1.982	1.602	1.623	1.860	2.780	1.120	2.692
$10^{2.0}=100.0$	0.379	0.363	0.276	0.255	0.618	2.113	1.600	1.624	1.860	2.780	1.121	2.891
$10^{2.5}=316.2$	0.379	0.363	0.276	0.255	0.618	2.099	1.600	1.624	1.859	2.780	1.119	2.891
$10^{3.0}=1000$	0.379	0.362	0.276	0.255	0.618	2.118	1.600	1.631	1.860	2.780	1.119	2.892

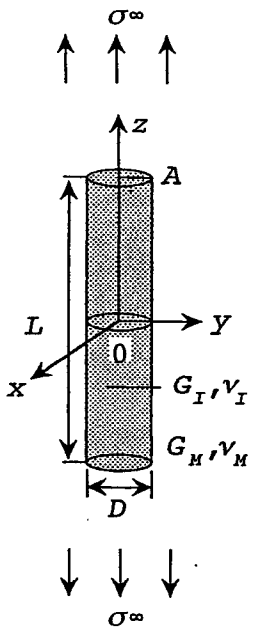

Table 4 F_{I,λ_1} and F_{II,λ_2} for a rectangular inclusion under uniaxial tension in the longitudinal direction, the case of plane strain, $\nu_M=\nu_I=0.3$

L/D \ G_I/G_M	F_{I,λ_1}						F_{II,λ_2}					
	10^{-5}	10^{-2}	10^{-1}	2	10^{1}	10^{2}	10^{-5}	10^{-2}	10^{-1}	2	10^{1}	10^{2}
$10^{0.0}=1.0$	0.591	0.555	0.368	0.198	0.230	0.244	2.208	2.226	2.415	2.386	0.531	0.439
$10^{0.5}=3.162$	0.540	0.511	0.359	0.240	0.359	0.413	2.044	2.060	2.233	2.581	0.707	0.646
$10^{1.0}=10.0$	0.513	0.489	0.351	0.258	0.495	0.673	1.968	1.979	2.135	2.741	0.944	1.018
$10^{1.5}=31.62$	0.502	0.484	0.348	0.264	0.593	1.064	1.938	1.944	2.099	2.804	1.137	1.619
$10^{2.0}=100.0$	0.498	0.484	0.347	0.265	0.635	1.544	1.940	1.930	2.083	2.825	1.224	2.377
$10^{2.5}=316.2$	0.497	0.483	0.346	0.266	0.649	1.893	1.924	1.931	2.084	2.831	1.248	2.933
$10^{3.0}=1000$	0.493	0.483	0.346	0.266	0.651	1.950	1.924	1.926	2.081	2.832	1.255	2.977

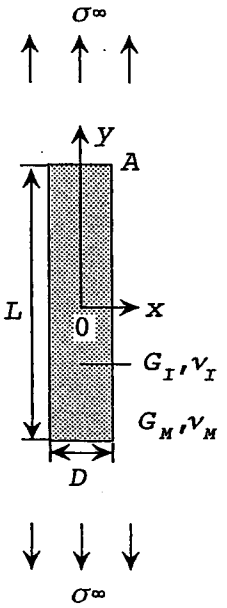

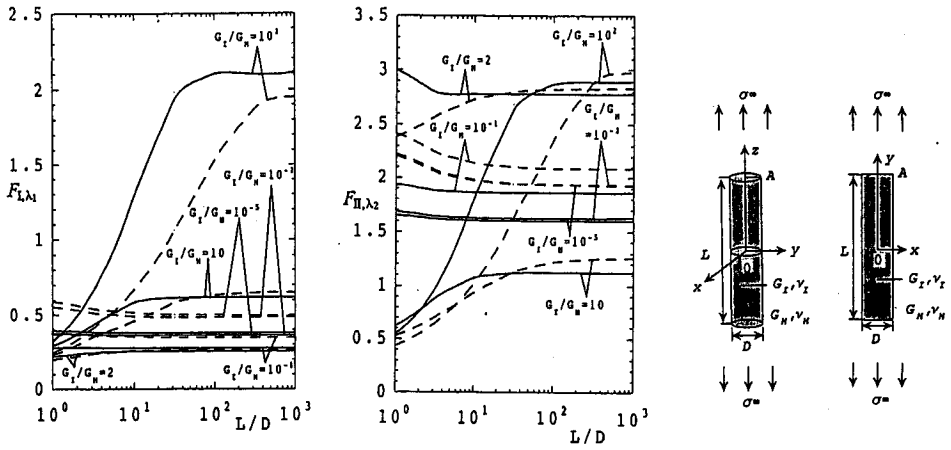

Fig. 4 F_{I,λ_1} and F_{II,λ_2} for a cylindrical inclusion (solid line) and a rectangular inclusion (broken line) under longitudinal tension ($\nu_M=\nu_I=0.3$)

stress intensity factors K_{I,λ_1}, K_{II,λ_2}, K_{III,λ_3}, K_{III,λ_4} for corner A can be obtained from the values of weight functions at the corner tip $W_n^I(0)$, $W_l^I(0)$, $W_n^{II}(0)$, $W_l^{II}(0)$, $W_\theta^{III,\lambda_3}(0)$, $W_\theta^{III,\lambda_4}(0)$. The expressions may be found in Nisitani et al. ([5]), and Noda et al. ([17]).

3 Numerical Results and Discussion

The generalized stress intensity factors K_{I,λ_1}, K_{II,λ_2}, K_{III,λ_3}, K_{III,λ_4} defined in Refs. [1], [2] are analyzed with varying the aspect ratio L/D and elastic ratio G_I/G_M. In the following discussion, dimensionless stress intensity factors $F_{I,\lambda_1}\sim F_{III,\lambda_4}$ are shown assuming Poisson's ratio $\nu_I=\nu_M=0.3$,

$$\begin{aligned} F_{I,\lambda_1}&=K_{I,\lambda_1}/\sigma^\infty\sqrt{\pi}(D/2)^{1-\lambda_1},\\ F_{II,\lambda_2}&=K_{II,\lambda_2}/\sigma^\infty\sqrt{\pi}(D/2)^{1-\lambda_2},\\ F_{III,\lambda_3}&=K_{III,\lambda_3}/\sigma^\infty\sqrt{\pi}(D/2)^{1-\lambda_3},\\ F_{III,\lambda_4}&=K_{III,\lambda_4}/\sigma^\infty\sqrt{\pi}(D/2)^{1-\lambda_4}. \end{aligned} \tag{6}$$

Convergence of the results are shown for the problem of pure shear in the xy plane in Fig. 1*d*. Table 1 shows the values of F_{I,λ_1}, F_{II,λ_2} at the corner $A(\theta=0)$ and the values of F_{III,λ_3} at the corner $A(\theta=\pi/4)$ for $L/D=10$, $G_I/G_M=10^2$. Also Table 2 shows the values of F_{I,λ_1}, F_{II,λ_2} at the corner $A(\theta=0)$ and the values of F_{III,λ_4} at the corner $A(\theta=\pi/4)$ for $L/D=10$, $G_I/G_M=10^{-5}$. In Tables 1 and 2, M is the number of collocation points at each boundary division, and the total number of collocation points is $7M$. As shown in Tables 1 and 2, The F_{I,λ_1} values can be determined from the values $W_{nM}^I(0)$, $W_{lM}^I(0)$, and the F_{II,λ_2} values can be determined from the values of $W_{nM}^{II}(0)$, $W_{lM}^{II}(0)$. From the examination as shown in Tables 1 and 2, we can see the following.

(1) When $G_I/G_M>1$, the difference of the F_{I,λ_1}, F_{II,λ_2} values obtained from different components of unknown functions $W_{nM}^I(0)$, $W_{lM}^I(0)$ is larger, about 10%. When $G_I/G_M<1$, the difference is smaller, about a few percent. Similar tendency was seen in the analysis of a 2D rectangular inclusion [4].

(2) The average values of F_{I,λ_1}, F_{II,λ_2}, which is obtained from different components, always have good convergence for $M=5$, 6 and look reliable.

(3) The values of F_{III,λ_3}, F_{III,λ_4} are only a few percent compared with the values of F_{I,λ_1}, F_{II,λ_2}.

(4) The final results are obtained without using extrapolation because the weight functions are approximated as power series instead of step or linear functions [3–5] used usually in the body force method. The convergence of the present solution is better than the cases of Nisitani [5] and Chen [3,4].

The following values of F_{I,λ_1}, F_{II,λ_2} are obtained confirming the convergence of the average values for various aspect ratio L/D and elastic ratio G_I/G_M.

In Table 3, the results for a cylindrical bar under uniaxial tension in the z direction are shown. For comparison, Table 4 shows the results for a rectangular inclusion under longitudinal tension obtained in the similar way of the present analysis. Chen's results [3] are in good agreement with Table 4. Results of Tables 3 and 4 are plotted in Fig. 4 as a comparison between the 3D and 2D models. With increasing the value L/D, the stress intensity factors increase and finally become saturated. For the same elastic ratio G_I/G_M, 3D and 2D results have a similar tendency with the difference under ±30% in most cases.

Table 5 shows the values of F_{I,λ_1}, F_{II,λ_2} at the corner $A(\theta=0)$, and Table 6 shows the ones at the corner $A(\theta=\pi/2)$ for uniaxial tension of a cylindrical inclusion in the x direction. Figures 5 and 6 are the plots of Tables 5 and 6. As shown in these tables and figures, the stress intensity factors have the largest values at $A(\theta=0)$ in most cases. From the comparison between the results of Figs. 4 and 5, it is found the F_{I,λ_1} values for z-directional tension are one to four times larger than the ones for x-directional tension in most cases, although the F_{II,λ_2} values are in the same order. From Figs. 4 and 5, it may be concluded that the stress intensity factors take saturated values at nearly the same value of L/D; for example, when $G_I/G_M=10^2$, the F_{I,λ_1} values become saturated when $L/D=100$ in Figs. 4 and 5. In Fig. 5, for high G_I/G_M, the stress intensity F_{I,λ_1} decreases with L/D, becomes almost zero at $L/D=10$, and then increases. Usually, F_{I,λ_1} increases with increasing L/D; however, as $L/D\to 1$, the interaction between both ends of the cylinder seems to make F_{I,λ_1} larger. In Fig. 6, when $G_I/G_M=10^2$ the stress intensity F_{I,λ_1} changes in sign as L/D increases, because in two auxiliary problems in Figs. 1*c* and *d*, F_{I,λ_1} depends on L/D differently. In Table 7 and Fig. 7 the results for a rectangular inclusion under transverse tension are shown. The difference between the results for Figs. 5 and 7 is very large, in other words, it seems difficult to use 2D solution to evaluate the 3D results if the load is applied in the transverse direction.

Table 5 F_{I,λ_1} and F_{II,λ_2} for a cylindrical inclusion at the corner A when θ=0 under uniaxial tension in the x direction ($\nu_I=\nu_M=0.3$)

G_I / G_M L / D	F_{I,λ_1}						F_{II,λ_2}					
	10^{-5}	10^{-2}	10^{-1}	2	10^{1}	10^{2}	10^{-5}	10^{-2}	10^{-1}	2	10^{1}	10^{2}
$10^{0.0}$=1.0	0.300	0.288	0.226	0.205	0.263	0.294	1.402	1.426	1.673	-3.278	-0.724	-0.624
$10^{0.5}$=3.162	0.302	0.290	0.226	0.193	0.206	0.186	1.317	1.342	1.587	-3.391	-0.833	-0.805
$10^{1.0}$=10.0	0.312	0.299	0.230	0.189	0.166	-0.019	1.280	1.305	1.550	-3.431	-0.898	-1.058
$10^{1.5}$=31.62	0.313	0.300	0.231	0.188	0.165	0.572	1.274	1.299	1.544	-3.442	-0.917	-1.314
$10^{2.0}$=100.0	0.313	0.300	0.231	0.188	0.166	0.614	1.274	1.299	1.544	-3.442	-0.918	-1.371
$10^{2.5}$=316.2	0.314	0.300	0.231	0.188	0.164	0.615	1.274	1.298	1.544	-3.443	-0.918	-1.373
$10^{3.0}$=1000	0.314	0.300	0.231	0.188	0.164	0.616	1.274	1.298	1.544	-3.443	-0.918	-1.373

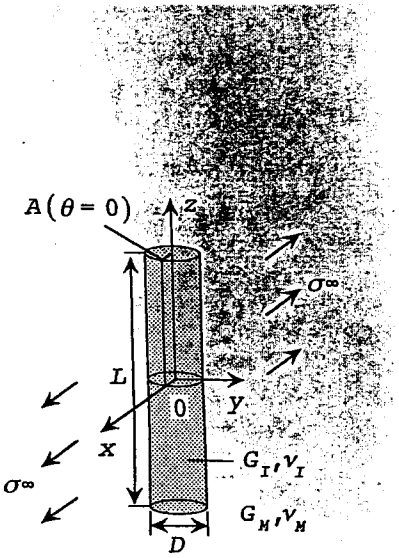

Table 6 F_{I,λ_1} and F_{II,λ_2} for a cylindrical inclusion at corner A when $\theta=\pi/2$ under uniaxial tension in the x direction

G_I / G_M L / D	F_{I,λ_1}						F_{II,λ_2}					
	10^{-5}	10^{-2}	10^{-1}	2	10^{1}	10^{2}	10^{-5}	10^{-2}	10^{-1}	2	10^{1}	10^{2}
$10^{0.0}$=1.0	0.067	0.062	0.033	-0.019	-0.068	-0.091	0.160	0.160	0.164	0.168	0.080	0.069
$10^{0.5}$=3.162	0.083	0.077	0.041	-0.022	-0.103	-0.171	0.241	0.242	0.246	0.217	0.060	-0.018
$10^{1.0}$=10.0	0.093	0.086	0.045	-0.027	-0.145	-0.379	0.228	0.229	0.233	0.191	0.000	-0.269
$10^{1.5}$=31.62	0.095	0.087	0.046	-0.027	-0.146	0.212	0.222	0.223	0.227	0.180	-0.019	-0.525
$10^{2.0}$=100.0	0.095	0.087	0.046	-0.027	-0.145	0.254	0.222	0.223	0.227	0.180	-0.020	-0.582
$10^{2.5}$=316.2	0.095	0.087	0.046	-0.027	-0.146	0.255	0.222	0.222	0.227	0.179	-0.020	-0.584
$10^{3.0}$=1000	0.095	0.087	0.046	-0.027	-0.146	0.256	0.222	0.222	0.227	0.179	-0.020	-0.584

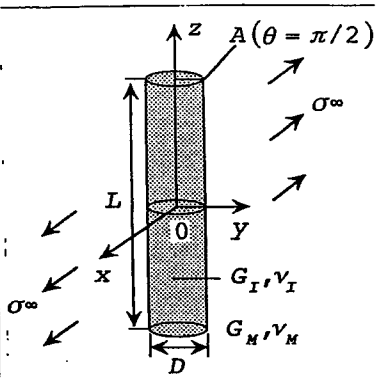

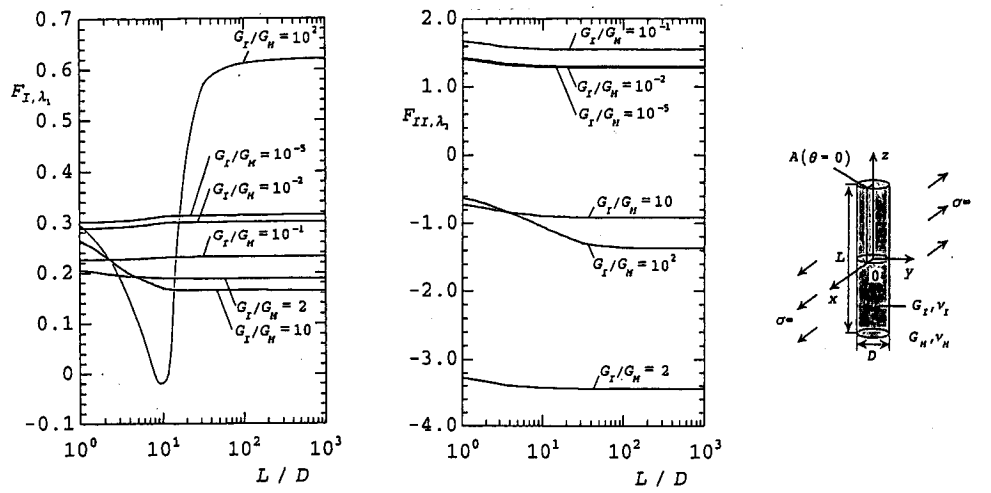

Fig. 5 F_{I,λ_1} and F_{II,λ_2} for a cylindrical inclusion under uniaxial tension in the x direction (at corner A with $\theta=0$, $\nu_M=\nu_I=0.3$)

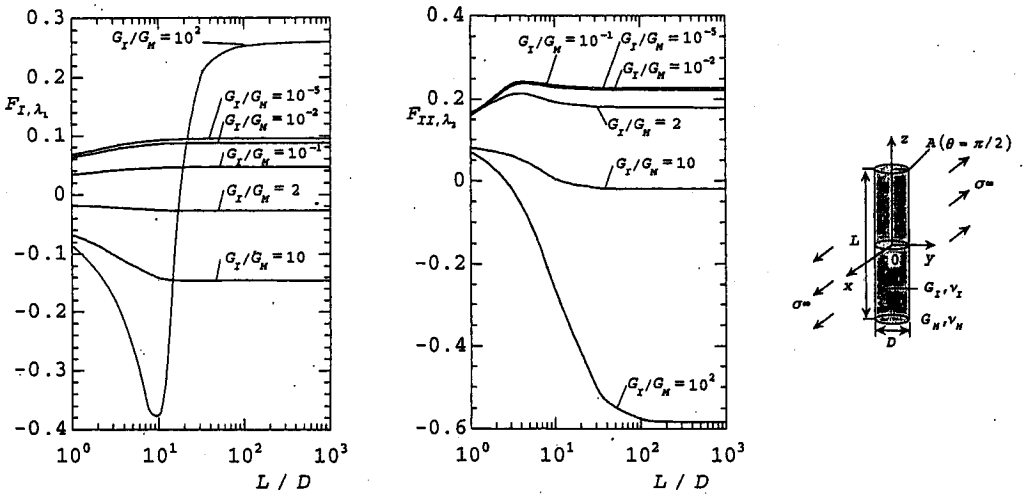

Fig. 6 F_{I,λ_1} and F_{II,λ_2} for a cylindrical inclusion under uniaxial tension in the x direction (at corner A with $\theta=\pi/2$, $\nu_M=\nu_I=0.3$)

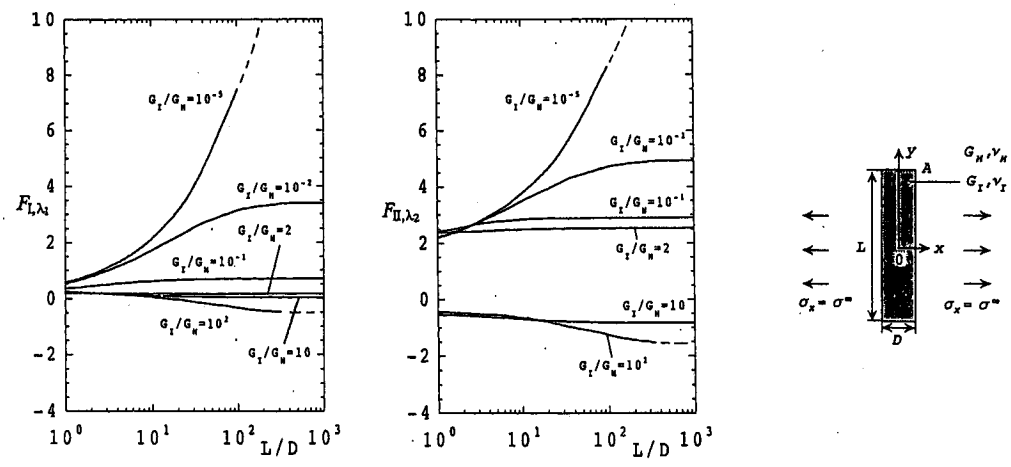

Fig. 7 F_{I,λ_1} and F_{II,λ_2} for a rectangular inclusion under transverse tension, the case of plane strain $\nu_M=\nu_I=0.3$

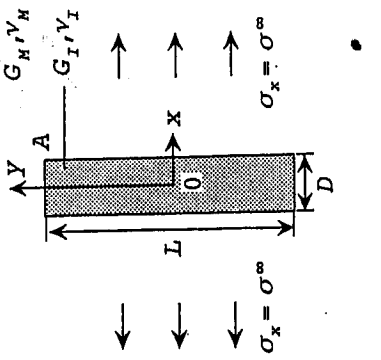

Table 7 F_{I,λ_1} and F_{II,λ_2} for a rectangular inclusion under transverse tension, the case of plane strain $\nu_M = \nu_I = 0.3$

	F_{I,λ_1}						F_{II,λ_2}					
L/D \ G_I/G_M	10^{-5}	10^{-2}	10^{-1}	2	10^{1}	10^{2}	10^{-5}	10^{-2}	10^{-1}	2	10^{1}	10^{2}
$10^{0.0}=1.0$	0.591	0.555	0.368	0.198	0.230	0.244	2.208	2.226	2.415	2.386	-0.532	-0.439
$10^{0.5}=3.162$	1.124	1.007	0.517	0.176	0.167	0.165	2.798	2.777	2.719	2.427	-0.595	-0.518
$10^{1.0}=10.0$	2.148	1.741	0.628	0.165	0.103	0.051	3.774	3.505	2.856	2.494	-0.696	-0.634
$10^{1.5}=31.62$	4.052	2.595	0.678	0.159	0.057	-0.122	5.423	4.263	2.892	2.524	-0.776	-0.929
$10^{2.0}=100.0$	7.484	3.169	0.692	0.158	0.038	-0.330	8.279	4.738	2.902	2.533	-0.815	-1.254
$10^{2.5}=316.2$	-	3.390	0.697	0.158	0.032	-0.484	-	4.920	2.903	2.532	-0.826	-1.500
$10^{3.0}=1000$	-	3.390	0.697	0.158	0.032	-	-	4.920	2.903	2.536	-0.826	-

4 Conclusion

In this paper, a cylindrical inclusion as a 3D model of a short fiber in composites was analyzed. Using the body force method the problem is formulated as singular integral equations. The generalized stress intensity factors are calculated with varying the aspect ratió L/D and elastic ratio G_I/G_M. The conclusions can be made as follows.

(1) In the numerical solution of the singular integral equations of the body force method, the unknown functions were approximated by the products of the fundamental density functions and the power series along the short segments into which whole boundary is discretized. The convergence of the present solution is better than the cases of Nisitani [5] and Chen [3,4], where the final results are obtained by using extrapolation. The average values of F_{I,λ_1}, F_{II,λ_2}, which is obtained from different components of unknown functions, always have good convergence to the third digit, and look reliable, even for the collocation number of each division $M=5$, 6. The results are shown in the tables and figures.

(2) When the cylindrical inclusion under z-directional tension the F_{I,λ_1} values are one to four times larger than the ones when the cylindrical inclusion under x-directional tension in most cases although the F_{II,λ_2} values are almost in the same order.

(3) From the comparison between the results of a 3D cylindrical inclusion and a 2D rectangular inclusion, it appears though 3D and 2D results have a similar tendency with the difference under ±30% in most cases when the load is applied in the longitudinal direction. However, the difference is very large if the load is applied in the transverse direction. Care should be taken if the 2D solution is applied to evaluate the 3D results.

(4) The values of F_{III,λ_3}, F_{III,λ_4} are only a few percent compared with the values of F_{I,λ_1}, F_{II,λ_2}.

Acknowledgments

This research was supported by the Kyushu Institute of Technology Fellowship, and the Japan Society for the Promotion of Science Postdoctral Fellowship. The authors wish to express their thanks to the members of their group, especially Mr. T. Morodomi and Mr. Y. Kumagae, who carried out much of the constructional work.

Appendix: How to Evaluate Singular Integrals

In this analysis it is important to evaluate integrals in Eqs. (1*a*) and (1*b*) accurately because they have singularities when the integral interval includes boundary collocation points. In the previous studies these integrals were evaluated as shown in the following way [6,18]. The integral interval is divided into three parts as shown in Fig. 3*b* and Eq. (6),

$$I=\int_a^b f(x)dx=\int_a^{\varepsilon-\varepsilon_0} f(x)dx+\int_{\varepsilon-\varepsilon_0}^{\varepsilon+\varepsilon_0} f(x)dx+\int_{\varepsilon+\varepsilon_0}^{b} f(x)dx$$
$$=I_1+I_2+I_3. \tag{A1}$$

If we take suitable small values of $2\varepsilon_0$ the integral I can be evaluated as Eq. (*A*2),

$$I=\int_{-\varepsilon_0}^{\varepsilon_0} f(x)dx$$
$$=\int_{-\varepsilon_0}^{\varepsilon_0}\left(\frac{C_{-1}}{\varepsilon}+C_0+D_0\ln|\varepsilon|+C_1\varepsilon+D_1\varepsilon\ln|\varepsilon|\right.$$
$$\left.+D_1\varepsilon^2\ln|\varepsilon|+\cdots\right)$$
$$=2C_0\varepsilon_0+2D_0(\varepsilon_0\ln\varepsilon_0-\varepsilon_0). \tag{A2}$$

Here, C_{-1}, C_0, D_0 are constants, which may be obtained from expansion forms around $x=\varepsilon$ with painstaking tasks. In this study therefore the following method is applied. First, we set

$$I_{2\varepsilon}=I-\int_{-\varepsilon_0}^{\varepsilon_0} f(\varepsilon)d\varepsilon, \quad I_{4\varepsilon}=I-\int_{-2\varepsilon_0}^{2\varepsilon_0} f(\varepsilon)d\varepsilon,$$

$$I_{8\varepsilon}=I-\int_{-4\varepsilon_0}^{4\varepsilon_0} f(\varepsilon)d\varepsilon. \tag{A3}$$

These integrals can be expressed by

$$I_{2\varepsilon}=I-2C_0\varepsilon_0-2D_0(\varepsilon_0\ln\varepsilon_0-\varepsilon_0)=I-C'-D'\varepsilon_0\ln(2\varepsilon_0),$$

$$I_{4\varepsilon}=I-2C'\varepsilon_0-D'(2\varepsilon_0)\ln(2\varepsilon_0), \tag{A4}$$

$$I_{8\varepsilon}=I-4C'\varepsilon_0-D'(4\varepsilon_0)\ln(4\varepsilon_0),$$

where $C'=2(C_0-D_0)$, $D'=2D_0$. Since the integrals $I_{2\varepsilon}$, $I_{4\varepsilon}$, $I_{8\varepsilon}$ exclude singular points, they can be evaluated accurately through normal numerical procedure. Finally, we can evaluate I from

$$I=4I_{2\varepsilon}-4I_{4\varepsilon}-I_{8\varepsilon}. \tag{A5}$$

References

[1] Chen, D. H., and Nisitani, H., 1991, "Singular Stress Fields at a Corner of Jointed Dissimilar Material Under Antiplane Loads," Trans. Jpn. Soc. Mech. Eng., Ser. A, **57**-542, pp. 2499–2503 (in Japanese) [1992, JSME Int. J., Ser. I, **35**-4, pp. 399–403].

[2] Chen, D. H., and Nisitani, H., 1993, "Singular Stress Near the Corner of Jointed Dissimilar Materials," Trans. ASME, J. Appl. Mech., **60**, pp. 607–613.

[3] Chen, D. H., 1992, "Analysis for Corner Singularity in Composite Materials Based on the Body Force Method," *Localized Damage II*, Vol. 1, pp. 397–421.

[4] Chen, D. H., and Nisitani, H., 1992, "Analysis of Intensity of Singular Stress Fields at Fiber End," Trans. Jpn. Soc. Mech. Eng., Ser. A, **58**-554, pp. 1834–1838 (in Japanese).

[5] Nisitani, H., Chen, D. H., and Shibuko, A., 1993, "Singular Stress at a Corner of Lozenge Inclusion Under Antiplane Shear," Trans. Jpn. Soc. Mech. Eng., Ser. A, **59**-561, pp. 1191–1195 (in Japanese).

[6] Nisitani, H., 1967, "The Two-Dimensional Stress Problem Solved Using an Electric Digital Computer," J. Jpn. Soc. Mech. Eng., **70**, pp. 627–632 [1968, Bull. JSME, **11**, pp. 14–23].

[7] Kasano, H., Matsumoto, H., and Nakahara, I., 1981, "Tension of a Rigid Circular Cylindrical Inclusion in an Infinite Body," Trans. Jpn. Soc. Mech. Eng., Ser. A, **47**-413, pp. 18–26 (in Japanese).

[8] Hasegawa, H., and Yoshiya, K., 1994, "Tension of Elastic Solid With Elastic Circular-Cylindrical Inclusion," Trans. Jpn. Soc. Mech. Eng., Ser. A, **60**-575, pp. 1585–1590 (in Japanese).

[9] Takao, Y., Taya, M., and Chou, T. W., 1981, "Stress Field Due to a Cylindrical Inclusion With Constant Axial Eigenstrain in an Infinite Elastic Body," ASME J. Appl. Mech., **48**, pp. 853–858.

[10] Hasegawa, H., Lee, V.-G., and Mura, T., 1992, "The Stress Fields Caused by a Circular Cylindrical Inclusion," ASME J. Appl. Mech., **59**, pp. 107–114.

[11] Wu, L., and Du, S., 1995, "The Elastic Field Caused by a Circular Cylindrical Inclusion-Part I," ASME J. Appl. Mech., **62**, pp. 579–584.

[12] Wu, L., and Du, S., 1995, "The Elastic Field Caused by a Circular Cylindrical Inclusion-Part II," ASME J. Appl. Mech., **62**, pp. 585–589.

[13] Noguchi, H., Nisitani, H., Goto, H., and Mori, K., 1987, "Semi-Infinite Body With a Semi-Ellipsoidal Pit Under Tension," Trans. Jpn. Soc. Mech. Eng., Ser. A, (in Japanese), **53**-488, pp. 820–826 [1989, JSME Int. J., Ser. I, **32**-1, pp. 14–22].

[14] Noda, N., and Tomari, K., 1997, "Fundamental Solution and its Application for Stress Analysis of Axisymmetric Body Under Asymmetric Uniaxial Tension," Bulletin of the Kyushu Institute of Technology, **67**, pp. 7–12.

[15] Bogy, D. B., and Wang, K. C., 1971, "Stress Singularities at Interface Corners in Bonded Dissimilar Isotropic Elastic Materials," Int. J. Solids Struct., **7**, pp. 993–1005.

[16] Noda, N.-A., and Matsuo, T., 1998, "Singular Integral Equation Method for Interaction Between Elliptical Inclusions," ASME J. Appl. Mech., **65**, pp. 310–319.

[17] Noda, N.-A., Kawashima, Y., Moriyama, S., and Oda, K., 1996, "Interaction of Newly Defined Stress Intensity Factors for Angular Corners in a Row of Diamond-Shaped Inclusions," Int. J. Fract., **82**, pp. 267–295.

[18] Noda, N.-A., 1984, "Stress Concentration Analysis for Notched Round Bar Under Torsion, Tension, and Bending," Ph.D. Dissertation, Kyushu University, pp. 50–64 (in Japanese).